Effects of thinning a forest stand on sub-canopy turbulence

Eric S. Russell[a], Heping Liu[a], Harold Thistle[b], Brian Strom[c], Mike Greer[d] and Brian Lamb[a]

[a] Laboratory for Atmospheric Research, Department of Civil and Environmental Engineering, Washington State University, Pullman, WA 99164, USA

[b] USDA Forest Service, Forest Health Technology Enterprise Team, Morgantown, West Virginia 26505, USA

[c] Research Entomologist, USDA Forest Service, Pineville, LA

[d] Entomologist, Pasco County Mosquito Control District, Odessa, FL

For submission to: Agricultural and Forest Meteorology

Correspondence: Heping Liu, Department of Civil and Environmental Engineering, Washington State University, Pullman, WA 99164, USA.

Tel: 509-335-1529; Fax: 509-335-7632; Email: heping.liu@wsu.edu

Keywords: Sub-canopy turbulence; stand thinning; wavelet spectra

Abstract

The density of a forest canopy affects the degree of influence of vegetation on the mean and turbulence flow fields. Thinning a forest *in situ* is difficult and expensive therefore many studies investigating the effects of changing canopy density have been done in wind tunnels or with modeling. Here, we analyze data collected at 0.13h, 0.83h, and 1.13h (canopy height; h = 21 m) as the surrounding loblolly pine stand was progressively thinned three times. The first thinning removed the understory and the two subsequent thinnings removed whole trees leading to a 60% reduction in the overall stand density. As the forest was thinned, turbulence and wind speed near the surface (0.13h) increased and became more connected with above the canopy (1.13h). The variation of the three-dimensional wind components increased for 0.13h when the understory was thinned. Turbulence at 0.83h and 1.13h increased when whole trees were removed (2^{nd} and 3^{rd} thinning). An increase in the peak spectral power of the 0.13h vertical velocity indicated an increase in the influence of larger eddies surviving through the canopy, but these did not affect the vertical turbulence or momentum transfer.

1 Introduction

The density of a forest stand impacts the local flow and thermal fields leading to complex interactions between canopy geometry, turbulent transport and biophysical effects (Albertson et al., 2001; Starkenburg et al., 2015). An increase (decrease) in the stand density increases (decreases) the amount of turbulence damping and momentum absorption (Pujol et al., 2013). For the densest canopies, the majority of momentum absorption occurs in upper parts of the canopy where the majority of the foliage resides, limiting the impact of the underlying surface roughness on the flow (Huang et al., 2013; Yue et al., 2007). As the stand density decreases, the flow transitions from the mixed layer analogy (Raupach et al., 1996) toward a more classical boundary layer with isolated roughness elements (Pietri et al., 2009; Poggi et al., 2004). However, the way this transition occurs and how sparse the canopy needs to be for this transition to occur is unknown.

Changing turbulence with canopy density creates a direct connection between the within-canopy turbulence, stand density, and depth into the canopy (Burns et al., 2011; Chamecki, 2013; Green et al., 1995; Russell et al., 2016). Measurements of the *in situ* vertical turbulence profile have been used to study leaf-on/leaf-off cycles (Lee et al., 2011; Staebler and Fitzjarrald, 2005) and from the effects of changing stand densities via comparisons of different forests with different canopy densities (Finnigan, 2000). However, studies with *in situ* measurements where the surrounding stand density is changed are rare outside of wind tunnels (Green et al., 1995; Thistle et al., 2011).

The change from a perturbed mixing layer (dense canopy) to a wall-bounded boundary layer with irregularly placed obstacles (Pietri et al., 2009; Poggi et al., 2004) is often investigated using the standard deviation, skewness, and kurtosis within the canopy. Above the canopy, these statistics are not as strongly affected (Finnigan, 2000; Novak et al., 2000; Poggi et al., 2004). For different canopy types and densities, these values show that the vertical profile of turbulence above the canopy under neutral stability converges when normalized by friction velocity (u_*) measured at the canopy top (h_c) (Finnigan, 2000; Raupach et al., 1996). Within the canopy, there is a wider variation within the turbulence and wind profiles based off the canopy type, density, and surrounding conditions. The variation in the turbulence statistics with increasing stand density can explain some of the variability in the within-canopy portions of the "family portraits" (Novak et al., 2000).

Changes in the stand density modulate the turbulent structures affecting the scalar and momentum transfer through the canopy (Poggi et al., 2004). Stability is the other major factor driving the structure of turbulence structures in the sub-canopy (Dupont and Patton, 2012a, 2012b; Patton et al., 2016; Su et al., 2004; Thomas et al., 2013). Even at the lowest stand densities considered in the cited literature, the turbulence profile is consistent with a canopy-influenced profile (Novak et al., 2000; Pietri et al., 2009). By staggering the alignment of the canopy within a wind-tunnel, Pietri et al. (2009) concluded that a staggered canopy reduces the canopy's porosity and enhances tree-wake interactions. This creates a more even foliage layer to absorb momentum and separate the within-canopy layer from the atmosphere above. Unlike row crops and aligned forests, a more even distribution of the vegetation does not have the same wind direction dependence (Chahine et al., 2014).

To the best of our knowledge from a literature search, two datasets have been compiled from *in situ* measurements of a thinned forest (excluding leaf-on/leaf-off comparisons). Green et al. (1995) presented results for three plots (0.8 hectares each) thinned at different densities within a larger forest. Their results showed that tree spacing and canopy density are major factors in modifying canopy turbulence; in sparser canopies, more wind can penetrate the canopy due to local variations in the canopy density producing a spatially variable wind field. Edburg et al. (2010) described aspects of canopy flow and dispersion for a circular, 1.13 hectares (60m radius) progressively thinned loblolly pine forest finding that the lower canopy density increases the wind speed and turbulence within the canopy accelerating plume dilution while decreasing plume meandering. Thistle et al. (2011) showed that the more open canopy allows for more interaction between the sub-canopy and free atmosphere enhancing mixing and the possibility of coupling with the loss of the understory. The understory increases the number of roughness elements near the surface with which the flow can interact. Effects of the overstory on the flow have been described (Bai et al., 2012, 2015; Lee et al., 2011) more thoroughly than the effects of the understory (Blanken, 1998).

In this work, we investigate the effect of changing forest density on turbulence structure using the data introduced in Edburg et al. (2010) and Thistle et al. (2011) to describe how changing the density through the understory differs from removal of whole trees. The data set presented here is unique as the data were collected within the same forest stand without moving the instruments while the stand was successively thinned (Thistle et al., 2011). Previous work using these data has focused mainly on impacts of the stand thinning on tracer dispersion. The objective for this work is to investigate the effects of a decrease in canopy density on the evolution of the mean turbulence structure and connection between within and above canopy measurements as canopy density decreases.

2 Data and Methods

2.1 Data Site

Measurements were recorded at 10-Hz at three heights on the same tower (0.13h, 0.83h, and 1.13h; where h = 21 m was the average stand height) using Vx Probe sonic anemometers (Applied Technologies, Inc., Longmont, CO) in a loblolly pine forest near Winnfield, Louisiana USA (Winn Ranger District, Kisatchie National Forest; 31° 53′ 23.3″ N, 92°50′ 39.9″ W, Figure 1). Data were collected in the morning to early afternoon from May 14 to May 28, 2004 coinciding with the tracer releases (Thistle et al., 2011). Over the study period, the forest was thinned three times (Table 1) at a radius of 60 m leading to a total thinned area of 1.13 hectares (Thistle et al., 2011). Whether the fetch was long enough for the flow to reach a new equilibrium with the changed canopy density is unknown. The first thinning (T1) removed the understory which consisted of brush and red maple saplings, some of which extended up into the upper canopy. During the other two thinning periods (T2, T3), whole trees were removed by a heavy tractor with a grapple able to manipulate the removed trees. The measurement tower was not disturbed during this process so the sonic anemometers maintained a consistent set-up. Mean meteorological data were collected from the nearest airport station at Natchitoches, LA (KIER) located approximately 30 km southwest of the measurement site. For more details regarding the experimental set-up and tracer-dispersion results see Thistle et al. (2011).

The sonic anemometer data used here were collected between 12:00 UTC and 20:00 UTC. Data were pre-processed by despiking (Vickers and Mahrt, 1997) and checked against the instrument measurement limits. No coordination rotations were performed to preserve the effect of changing canopy geometry on the 3-dimensional flow components. Hereafter, u, v, w, and V refer to the longitudinal, lateral, vertical, and mean streamwise winds ($V = [u^2 + v^2]^{1/2}$), respectively. Data were block averaged for the entirety of each thinning period. The statistics in

Section 3.1 were calculated from the 100 second averages. Following convention, 30-minute averages were used to calculate the stability metrics presented in Section 3.2.

A RemTech PA0 SODAR (Remtech, Inc., Velizy France) was located approximately 2 km west of the tower site in a clearing (Figure 1) and operated from May 15 to 27, 2004. The SODAR measured 15 min mean horizontal wind speed and direction at 20 m increments from 20 to 600 m over the same period as the sonic anemometer collected data. Only data collected from 20 to 400 m above ground level were used due to the sparse data above 400 m.

2.2 Global Wavelet Transform

Overall, 177 half-hour periods were measured. Of these, 15 were incomplete half-hours leaving a total of 162 full half-hour data blocks. Mean global wavelet spectra were calculated from 30-minute blocks for each thinning and height. The 10 Hz data were block averaged to 1 Hz before the wavelet transform was calculated using a Morlet mother wavelet (Terradellas et al., 2001, 2005; Torrence and Compo, 1998). Spectral powers were normalized by the respective components' standard deviation (σ_x) (where x represents the u, v, and w components). The frequency was normalized by the mean streamwise wind speed (V) at each height and the height of the canopy (h_c). Hereafter, normalized frequencies are referred to as "n" ($n = fh_c/V$) and the natural frequencies as "f". Reported slopes were determined between the peak spectral energy and the spectral energy 1.5 decades times the frequency of the peak spectral energy except for T1 at 1.13h. The peak for T1 at 1.13h occurred before the roll-off so the peak before the roll-off was used as the starting point.

3 Results

3.1 Synoptic Conditions

A cold front moved through the northern and western portion of Louisiana between May 14 and May 15, stalling out over the eastern portion of the state on the border with Mississippi on May 16 (Figure 2). By 7 am Eastern Standard Time on May 17, the front had passed out of the region, leaving the measurement site under the influence of a high-pressure system. No other surface-based synoptic feature passed through the region during the measurement period. The high-pressure system kept the low-level SODAR-based wind direction consistent for the rest of the study period (Figure 3).

The wind direction shifted from approximately 135 degrees to between 225 and 315 degrees between May 16 and May 17, one day before the transition from UT to T1. This kept the SODAR upwind of the measurement site from May 17 onward. T2 and T3 had similar mean wind speed profiles after increases from UT to T1 to T2. Approximating $\mathrm{u}_* = \mathrm{kz}\frac{\partial \mathrm{u}}{\partial \mathrm{z}}$, where k is the von Karman constant (0.4), z is the measurement height, and $\frac{\partial \mathrm{u}}{\partial \mathrm{z}}$ is the vertical wind speed gradient, an estimate for the friction velocity (u_*) can be determined for each thinning within the canopy roughness layer. The canopy roughness layer is estimated to range between 2-5 times the canopy height (40-100 m here) (Hammerle et al., 2007; Thomas, 2011). With an inflection point observed in the SODAR data, we used the wind speeds between 60-200 m from the SODAR for the u_* estimation. In this zone, u_* was similar for UT to T2 at 1.13h, ranging between 0.55 m s^{-1} to 0.58 m s^{-1}, and it increased to 0.77 m s^{-1} for T3. The SODAR-based u_* values were similar with u_* at 1.13h (UT: 0.50 m s^{-1}, T1: 0.54 m s^{-1}, T2: 0.71 m s^{-1}, T3: 0.79 m s^{-1}) so the turbulence level just above the canopy was consistent with the broader canopy roughness layer.

3.2 Mean statistics and flow field

The distributions for the *u*- and *v*-components at 0.13h were similar through each thinning whereas distribution of the horizontal components at 1.13h changed from UT to T3 (Table 2, Figure 4). This was in part due to the changing synoptic conditions per Section 3.1 (Table 1). Changes in the distribution of the 0.83h horizontal components resembled 1.13h though the distribution of *w*-component was more similar to 0.13h. The *w*-component distribution at 1.13h changed minimally from UT to T3. At 0.13h, *w* was still centered near-zero but broadened with reduced skew and kurtosis from UT to T3. The loss of the understory (UT to T1) did not affect the distribution of the vertical velocity at 0.13h or 0.83h. As the canopy was thinned (T2 and T3), the skew and kurtosis of the horizontal wind fields became more similar among all the heights. There was a decreasing trend in the kurtosis values as the canopy density was reduced. Even with a sparser canopy, *w* was constrained within a narrower distribution at 0.13h and 0.83h compared to 1.13h.

3.3 Mean vertical profiles and stability

Overall, the mean flow at 0.13h did not change relative to 0.83h with each thinning (Figure 5a, 5b). The vertical velocities at each height presented relatively minimal change through each thinning (Table 2). Mean *V* increased with each thinning though mostly in the *u*-component (Figure 5a). Larger gains in *V* occurred at T2 and T3 when whole trees were removed from the canopy. The overlying wind speeds increased through the study period (Figure 3), which partially accounted for the change of wind speed at 1.13h independent of the canopy effects (Table 2). From UT to T1, all the standard deviations at 0.13h increased, suggesting less filtering of the variation within the mean wind. The lack of change in the standard deviations at 0.83h and 1.13h from UT to T1 indicates removing the understory only affected the results at 0.13h. For T2 and T3. The standard deviations at each height increased as the momentum absorption by the foliage was reduced and the overlying wind speed increased. The standard deviation in each flow component increased with each thinning (Figures 5d-f). From UT to T1, σ_u and σ_v increased relatively more than σ_w at 0.13h while there was some increase in all three standard deviations at 1.13h. AT 0.83h, σ_w decreased from UT to T1 and increased through to T3.

Comparing the change in V and u_* for each height at each half-hour from the sonic anemometer data (y-value) with the SODAR mean wind (x-value) shows the influence of the changing overlying wind speed in conjunction with the canopy thinning (Figure 6). From UT to T1, the slope (via an ordinary least squares regression) changed for 0.13h but less so at the other heights (Table 3). The consistency of the slope at 0.83h and 1.13h for both u_* and V across the period shows the general control of the synoptic wind speeds on the upper two heights. The slope change, lower R^2, and data (Figure 6) suggest a lower degree of control of the overlying winds at 0.13h for UT and T1 compared to T2 and T3. Scatter of the data reduced deeper in the canopy following the distribution from Section 3.2 and deeper in the canopy had a lower range of wind speed and turbulence across the same range of synoptic scale winds. The UT points with higher wind speeds that exhibited lower V and u_* values were the reason for the negative R^2 for UT. From T1 onward, the increases in the SODAR mean wind coincided with increases in u_* and V. From May 17 onward, the SODAR was generally upwind of the site and its data represent the inflow to the site.

Given the timing of the data, stability was plotted in three ways to account for different aspects of stability: the vertical virtual sonic temperature gradient ($d\theta_v/dz$), z/L, (where $L = \frac{\theta_v u_*^3}{kg\overline{w'\theta'}}$ is the Obukhov length and z was the measurement height), and the flux Richardson number ($Ri_f = \frac{g}{\theta_v}\frac{\overline{w'\theta'}}{\overline{w'V'}\left(\Delta V/\Delta z\right)}$) (Figure 4). The upper layer (1.13h to 0.83h) was generally positive for $d\theta_v/dz$ while the in-canopy layer (0.83h to 0.13h) was mostly negative for $d\theta_v/dz$ (Figure 7a and 7b). However, overall for each thinning, each height was generally unstable by way of z/L (Figure 7c and 7d) and dynamically unstable through the flux Richardson number (Figure 7e and 7f). Admittedly, z/L is not the best metric for forest and weak-wind, low turbulence stability characterization (Vickers and Mahrt, 2003; Williams et al., 2013). From Ri_f, we can gauge the relative contribution of the buoyant and mechanical terms to the overall level of turbulence along with stability (Stull, 1988). Ri_f was primarily negative, with smaller values in the 0.13h-0.83h layer compared to higher in the canopy indicating more similar thermal and mechanical contributions lower in the canopy compared to the upper layer. The upper layer used here goes through the top-of-canopy shear layer. All three metrics were relatively less variable with the sparser canopies (T2 and T3) as the penetration of net radiation and turbulence is more likely.

With the change in canopy density, the relationship between turbulence and stability became more constant within each height (Figure 8). For UT, there was some scatter in σ_w with $d\theta_v/dz$ which was not apparent in T1 forward (Figures 8a, 8c, and 8e). The increase in σ_w with increase in the temperature gradient was consistent across each thinning and height, the larger σ_w values occurred with the larger temperature gradient. With respect to the local z/L (Figures 8b, 8d, and 8f), a similar pattern was observed. As the canopy density was reduced, the z/L values were more concentrated closer to zero and the levels of σ_w were generally higher. 0.13h still exhibited some of the same scatter for T3 as UT (Figure 8f) so the canopy was still dense enough there to maintain some impact on stability deeper in the canopy, consistent with what was observed in Figure 7.

3.4 Comparison to other Studies

The vertical profile of friction velocity (u_*) was plotted as a reference for the level of turbulence for each thinning at each height (Figure 9a). The normalizations were accomplished with the relevant value at 1.13h and the results from this work were compared to those from several previous studies (e.g., Finnigan, 2000; Green et al., 1995; Novak et al., 2000; Raupach et al., 1996). Changes in canopy density did not have a strong effect on the normalized horizontal flow field (Figures 9b-9f). Values of σ_w/u_* fell outside the range of values from other studies (shading in Figure 9) for 0.83h and 1.13h (Figure 9c). The normalized horizontal flow variations (σ_v/u_*) were consistent with previous studies (Figure 6d). Normalized momentum transfer ($\overline{w'V'}/u_*^2$, Figure 9e) and R_{wV} ($R_{wV} = \frac{\overline{w'V'}}{\sigma_w \sigma_V}$, Figure 9f) at 0.83h and 1.13h likewise fell near the edges of the ranges from previous studies. This is a result of the normalization height being above the canopy instead of at the canopy top as in the cited literature. As some correlation existed in the horizontal wind (R_{uv} = 0.24-0.38) even with minimal R_{wV}, this supports the idea of the flow “sloshing” near the surface without being transported vertically (Boldes et al., 2007).

The shear length scale ($Ls = {V_h}/{(\Delta V/\Delta z)}$) normalized by canopy height (Ls/h_c) increased from 0.44 for UT to 0.58 for T3 (T1 = 0.46 and T2 = 0.49). The increase and magnitude of Ls/h_c with decreased canopy density is consistent with previous studies (Finnigan, 2000; Raupach et al., 1996). Since the mean tree spacing did not change between UT and T1, the value of Ls/h_c should remain similar.

Viewing these results in context with the varying synoptic conditions (Sections 3.1 and 3.3), we can infer that synoptic conditions had less influence on the range of the normalization within a “family portrait” style plot than thinning (Figure 9), especially given the consistency of the relations between the overlying wind speed with u_* (Table 3). The variety of tree species and canopy densities represented by the cited studies as well as the similarities of the results suggest that tree type and density do not have a strong influence over the mean vertical profile of sub-canopy and near-canopy normalized values.

3.5 Wavelet turbulence structure

For UT at 0.13h, the characteristic spectral short-circuiting (SSC) pattern was observed without the secondary high frequency maximum (Figure 10) which is often associated with wake production behind trees (Dupont et al., 2012; Green et al., 1995). SSC manifests as a faster roll-off from peak frequencies to higher frequencies compared to the -2/3 power law (Cava and Katul, 2008). The slope for the *u*- and *v*-spectra at 0.13h decreased from -1.25 and -1.23 for UT, respectively, and to -1.0 and -0.84, respectively, for T3. At 1.13h, the slopes varied between -0.62 and -0.71 across the period, consistent with the -2/3 power law as observed in other canopies (Blanken, 1998; Finnigan, 2000; Liu et al., 2001; Van Gorsel et al., 2003). The shape of the 0.83h spectra was similar to the shape of the 1.13h spectra, but the slope at 0.83h decreased from UT for both *u* (-0.67) and *v* (-0.64) to T3 (u = -0.43 and v = -0.49). The peak *w*-spectral powers for both 1.13h and 0.83h did not vary much between each thinning (±0.2) with the peak frequency being relatively stable for 1.13h with *n* between 0.33 and 0.36. At 0.83h, *n* shifted from 0.59 for UT to 0.78 for T3. At 0.13h, the shift in peak *w*-spectra power was akin to the upper two heights (UT = 2.37 to T3 = 2.58) but more dramatic for the normalized frequency from n = 0.51 at UT to n = 1.25 at T3.

The slopes for the *w*-spectra at 1.13h changed from -0.76 (UT) to -0.66 (T3) and 0.83h from -0.74 (UT) to -0.77 (T3) indicating a less steep roll-off of energy with the decreased canopy density and increased overlying turbulence compared to 0.13h. The slopes for the *w*-spectra at 0.13h increased from UT (-0.44) to T3 (-0.59) indicating a slower initial loss of energy for vertically orientated structures compared to above the canopy and a transition toward a more consistent slope across all heights. For all the heights, the low frequency (pre-spectral peak) portion of the horizontal spectra smoothed out as the canopy density was reduced.

With the denser understory for UT, small-scale structures can be confounded due to overlapping scales of interactions from the different obstacle sizes (Bai et al., 2015). The combination of the wind speed and diameter of the trees (*d*) pushes the potential vortex-shedding frequency (f_{vs}) via the Strouhal number ($St = \frac{(f_{vs} * d)}{V}$) to frequencies smaller than what was measurable with this set-up (Cava and Katul, 2008; Dupont et al., 2012). The resolution of the sonic from its path-length (15 cm) and precision (0.01 m s^{-1}) limit its ability to measure eddies smaller than 15 cm (sonic path length). This is equivalent to frequencies in the range of 5-10 Hz from the measured mean winds. The diameter of an obstacle to produce an eddy of at least 5 Hz at these wind speeds is then between 0.05-0.1 m. Since the data were averaged to 1Hz prior to the transform, this shifted the diameter of an obstacle that could produce a measurable wake structure to approximately 0.4 m or larger when V= 2 m s^{-1}. With the measurement set-up and data processing utilized here; the small-scale wakes that are often reported through this type of analysis would not be visible within our data due to the sonic's path-averaging.

4 Discussion

Removing the understory (UT to T1) but retaining the overstory did not have a noticeable impact on the turbulence profile above 0.13h. If the understory were removed last instead of first, the changes in turbulence at 0.13h may have been different as the smaller obstacles would have remained and kept the near-surface canopy density relatively high compared to the rest of the canopy. Reducing the canopy density reduced the absorption of the variation in the flow field by the canopy elements and increased the amount of momentum transported through the canopy through reduced drag influence (Sun et al., 2006). However, the flow at 0.13h is not entirely driven by top-down momentum transfer (Staebler and Fitzjarrald, 2005) so flow in the lower canopy is not entirely reliant on transport from above the canopy. There was a proportional change between the mean u_* and wind speed so the normalized profiles did not show change much with each thinning. The general similarity with the previous studies and across each thinning with the changing overlying wind speed shows that the normalized profiles do not have a strong dependence on the above-canopy wind speed as they are directly related through the roughness of the surface.

With the thinning of the canopy, the similarities between 0.13h and 1.13h increased in the mean flow and turbulence relationship but there remained some differences in the turbulence structure. From UT to T1, removal of the understory eliminated the effects of small obstacles leaving interactions primarily with the larger obstacles, changing the shape of the *w*-spectra (Figure 10i). The horizontal spectra at 0.13h were similar at both UT and T1 as the effects of the understory on the spectra were too small to be measurable. Individual tree branches are not as thick as the tree trunks so any flow-interaction effects would be at scales too small to be captured by sonic anemometers or confounded by multiple interactions (Bai et al., 2015). However, sufficiently thick clumps of branches or needles may convey a similar effect as the trunk. The peak spectral power across each thinning remained relatively consistent though there was an increase in the turbulence level and length scale as the canopy was thinned.

The change of the slope the horizontal spectra at 0.13h from UT to T3 indicates some change in the size of the eddies and structures nearest the surface with the changing stand density. By T3, the *u* and *v* spectra at 0.13h began to resemble those at the upper two heights. But the SSC shape remained, thus, even at a 60% reduction in the forest density, there were enough interactions with tree trunks proximate to the measurement point to affect the shape of the horizontal 0.13h spectra. An increase in the vertical velocity spectral power is consistent with an increase in the length scale and reduction in the interaction of the flow with the vegetation as the spacing within the canopy increases (Green et al., 1995) but occurred only after the understory was thinned. Deeper in the canopy, turbulence is better defined by smaller scale structures (Chamecki, 2013; Nepf et al., 2007; Poggi et al., 2004) mostly incapable of exchanging air with above the canopy. Opening of the tree spacing increases the potential penetration depth of structures into the canopy and the portion of the canopy "flushed" by larger, above canopy-based eddies (Chamecki, 2013).

Large eddies that could penetrate through the canopy can enhance the low frequency contribution to the variances and fluxes (Prabha et al., 2008) and potentially cause interactions between larger eddies and the locally generated turbulence (Gao et al., 2016). This manifest itself by the smoothing of the low frequency portion of the 0.13h and 0.83h spectra with each thinning. The increase in the potential mixing due to larger structures penetrating deeper into the canopy as a result of the reduction in density would aid in the dilution and transport of scalars (Cava and Katul, 2008; Thistle et al., 2011). Hence the increased dilution with decreased stand density described in Thistle et al. (2011) and Edburg et al. (2010) for this site resulted from increased turbulent mixing and exchange between within-canopy and above-canopy air.

5 Conclusions

The thinning of the forest had an impact on the turbulence structure but effects on the mean flow could not be separated from the changing synoptic conditions with the data available.

Thinning of the understory leaves tree trunks intact caused small changes in the horizontal spectra at 0.13h but affected the high frequency range of the vertical spectra at this height. The effects from UT to T1 did not translate to the rest of the canopy beyond 0.13h because only the near-surface vegetation density was affected. Thinning the whole canopy reduced the overstory, leading to increased mixing and a better coupling between the canopy layers and the atmosphere as larger eddies could penetrate through the canopy. The spectral slopes at 0.13h shifted toward -2/3 with each thinning while the upper two heights tended to be around this value during the whole period. The reduced canopy density created more consistent spectral and flow profiles across each height as the canopy became more porous to larger top-down structures. Multiple levels of eddy covariance measurements covering the entire day over longer time periods for each canopy density are needed to fully describe the effects of the changing canopy density and synoptic conditions on turbulence, stability, and fluxes.

Acknowledgements: We would like to acknowledge the work of Holly Peterson (Ret.) (Montana Technical University), Steve Edburg and Gene Allwine (Ret.) (Washington State University) and Scott Gilmour, Wes Throop, Jim Kautz (Ret.) and Mike Huey (Ret.) (USDA Forest Service, MTDC, Missoula, MT). We thank Robert Howell (Ret.), Frank Yerby (Ret.) for support and local arrangements as well as the remaining staff of the Winn District of the Kisatchie National Forest and Jim Meeker (USDA Forest Service, FHP, Pineville, LA). We thank the two anonymous reviewers for their constructive comments. This work was supported under USDA-FS-FHTET-FHP-TD.00.M03., USDA-FS-RWU-4501 and USDA-FS-Region 8, Forest Health Protection. H. Liu acknowledges support by National Science Foundation AGS under grants #1419614.

References

Albertson, J.D., Katul, G.G., Wiberg, P., 2001. Relative importance of local and regional controls on coupled water, carbon, and energy fluxes. Adv. Water Resour. 24, 1103–1118.

Bai, K., Katz, J., Meneveau, C., 2015. Turbulent Flow Structure Inside a Canopy with Complex Multi-Scale Elements. Bound.-Layer Meteorol. 155, 435–457. doi:10.1007/s10546-015-0011-2

Bai, K., Meneveau, C., Katz, J., 2012. Near-Wake Turbulent Flow Structure and Mixing Length Downstream of a Fractal Tree. Bound.-Layer Meteorol. 143, 285–308. doi:10.1007/s10546-012-9700-2

Blanken, P.D., 1998. Turbulent flux measurements above and below the overstory of a boreal aspen forest. Bound.-Layer Meteorol. 89, 109–140.

Boldes, U., Scarabino, A., Colman, J., 2007. About the three-dimensional behavior of the flow within a forest under unstable conditions. J. Wind Eng. Ind. Aerodyn. 95, 91–112. doi:10.1016/j.jweia.2006.05.005

Burns, S.P., Sun, J., Lenschow, D.H., Oncley, S.P., Stephens, B.B., Yi, C., Anderson, D.E., Hu, J., Monson, R.K., 2011. Atmospheric Stability Effects on Wind Fields and Scalar Mixing Within and Just Above a Subalpine Forest in Sloping Terrain. Bound.-Layer Meteorol. 138, 231–262. doi:10.1007/s10546-010-9560-6

Cava, D., Katul, G.G., 2008. Spectral Short-circuiting and Wake Production within the Canopy Trunk Space of an Alpine Hardwood Forest. Bound.-Layer Meteorol. 126, 415–431. doi:10.1007/s10546-007-9246-x

Chahine, A., Dupont, S., Sinfort, C., Brunet, Y., 2014. Wind-Flow Dynamics Over a Vineyard. Bound.-Layer Meteorol. 151, 557–577. doi:10.1007/s10546-013-9900-4

Chamecki, M., 2013. Persistence of velocity fluctuations in non-Gaussian turbulence within and above plant canopies. Phys. Fluids 1994-Present 25, 115110.

Dupont, S., Irvine, M.R., Bonnefond, J.-M., Lamaud, E., Brunet, Y., 2012. Turbulent Structures in a Pine Forest with a Deep and Sparse Trunk Space: Stand and Edge Regions. Bound.-Layer Meteorol. 143, 309–336. doi:10.1007/s10546-012-9695-8

Dupont, S., Patton, E.G., 2012a. Momentum and scalar transport within a vegetation canopy following atmospheric stability and seasonal canopy changes: the CHATS experiment. Atmospheric Chem. Phys. 12, 5913–5935. doi:10.5194/acp-12-5913-2012

Dupont, S., Patton, E.G., 2012b. Influence of stability and seasonal canopy changes on micrometeorology within and above an orchard canopy: The CHATS experiment. Agric. For. Meteorol. 157, 11–29. doi:10.1016/j.agrformet.2012.01.011

Edburg, S.L., Allwine, G., Lamb, B., Stock, D., Thistle, H., Peterson, H., Strom, B., 2010. A Simple Model to Predict Scalar Dispersion within a Successively Thinned Loblolly Pine Canopy. J. Appl. Meteorol. Climatol. 49, 1913–1926. doi:10.1175/2010JAMC2339.1

Finnigan, J., 2000. Turbulence in plant canopies. Annu. Rev. Fluid Mech. 32, 519–571.

Gao, Z., Liu, H., Russell, E.S., Huang, J., Foken, T., Oncley, S.P., 2016. Large eddies modulating flux convergence and divergence in a disturbed unstable atmospheric surface layer. J. Geophys. Res. Atmospheres 121, 2015JD024529. doi:10.1002/2015JD024529

Green, S.R., Grace, J., Hutchings, N.J., 1995. Observations of turbulent air flow in three stands of widely spaced Sitka spruce. Agric. For. Meteorol. 74, 205–225.

Hammerle, A., Haslwanter, A., Schmitt, M., Bahn, M., Tappeiner, U., Cernusca, A., Wohlfahrt, G., 2007. Eddy covariance measurements of carbon dioxide, latent and sensible energy fluxes above a meadow on a mountain slope. Bound.-Layer Meteorol. 122, 397–416. doi:10.1007/s10546-006-9109-x

Huang, S., Dahal, D., Singh, R., Liu, H., Young, C., Liu, S., 2013. Spatially explicit surface energy budget and partitioning with remote sensing and flux measurements in a boreal region of Interior Alaska. Theor. Appl. Climatol. 113, 549–560. doi:10.1007/s00704-012-0806-8

Lee, I.-H., Lee, Y.-H., Hong, J., 2011. Characteristics of canopy turbulence over a deciduous forest on complex terrain. Asia-Pac. J. Atmospheric Sci. 47, 281–291. doi:10.1007/s13143-011-0016-9

Liu, S., Liu, H., Xu, M., Leclerc, M.Y., Zhu, T., Jin, C., Hong, Z., Li, J., Liu, H., 2001. Turbulence spectra and dissipation rates above and within a forest canopy. Bound.-Layer Meteorol. 98, 83–102.

Nepf, H., Ghisalberti, M., White, B., Murphy, E., 2007. Retention time and dispersion associated with submerged aquatic canopies. Water Resour. Res. 43, W04422. doi:10.1029/2006WR005362

Novak, M.D., Warland, J.S., Orchansky, A.L., Ketler, R., Green, S., 2000. Wind tunnel and field measurements of turbulent flow in forests. Part I: uniformly thinned stands. Bound.-Layer Meteorol. 95, 457–495.

Patton, E.G., Sullivan, P.P., Shaw, R.H., Finnigan, J.J., Weil, J.C., 2016. Atmospheric Stability Influences on Coupled Boundary Layer and Canopy Turbulence. J. Atmospheric Sci. 73, 1621–1647. doi:10.1175/JAS-D-15-0068.1

Pietri, L., Petroff, A., Amielh, M., Anselmet, F., 2009. Turbulence characteristics within sparse and dense canopies. Environ. Fluid Mech. 9, 297–320. doi:10.1007/s10652-009-9131-x

Poggi, D., Porporato, A., Ridolfi, L., Albertson, J.D., Katul, G.G., 2004. The effect of vegetation density on canopy sub-layer turbulence. Bound.-Layer Meteorol. 111, 565–587.

Prabha, T.V., Leclerc, M.Y., Karipot, A., Hollinger, D.Y., Mursch-Radlgruber, E., 2008. Influence of Nocturnal Low-level Jets on Eddy-covariance Fluxes over a Tall Forest Canopy. Bound.-Layer Meteorol. 126, 219–236. doi:10.1007/s10546-007-9232-3

Pujol, D., Casamitjana, X., Serra, T., Colomer, J., 2013. Canopy-scale turbulence under oscillatory flow. Cont. Shelf Res. 66, 9–18. doi:10.1016/j.csr.2013.06.012

Raupach, M., Finnigan, J.J., Brunei, Y., 1996. Coherent eddies and turbulence in vegetation canopies: the mixing-layer analogy. Bound.-Layer Meteorol. 78, 351–382.

Russell, E.S., Liu, H., Gao, Z., Lamb, B., Wagenbrenner, N., 2016. Turbulence dependence on winds and stability in a weak-wind canopy sublayer over complex terrain. J. Geophys. Res. Atmospheres 2016JD025057. doi:10.1002/2016JD025057

Staebler, R.M., Fitzjarrald, D.R., 2005. Measuring canopy structure and the kinematics of subcanopy flows in two forests. J. Appl. Meteorol. 44, 1161–1179.

Starkenburg, D., Fochesatto, G.J., Cristóbal, J., Prakash, A., Gens, R., Alfieri, J.G., Nagano, H., Harazono, Y., Iwata, H., Kane, D.L., 2015. Temperature regimes and turbulent heat fluxes across a heterogeneous canopy in an Alaskan boreal forest: Spatial fluxes in a heterogeneous canopy. J. Geophys. Res. Atmospheres 120, 1348–1360. doi:10.1002/2014JD022338

Su, H.-B., Schmid, H.P., Grimmond, C.S.B., Vogel, C.S., Oliphant, A.J., 2004. Spectral characteristics and correction of long-term eddy-covariance measurements over two mixed hardwood forests in non-flat terrain. Bound.-Layer Meteorol. 110, 213–253.

Sun, H., Clark, T.L., Stull, R.B., Andrew Black, T., 2006. Two-dimensional simulation of airflow and carbon dioxide transport over a forested mountain. Agric. For. Meteorol. 140, 338–351. doi:10.1016/j.agrformet.2006.03.023

Terradellas, E., Morales, G., Cuxart, J., Yagüe, C., 2001. Wavelet methods: application to the study of the stable atmospheric boundary layer under non-stationary conditions. Dyn. Atmospheres Oceans, Mixing in Geophysical and Astrophysical Flows 34, 225–244. doi:10.1016/S0377-0265(01)00069-0

Terradellas, E., Soler, M.R., Ferreres, E., Bravo, M., 2005. Analysis of oscillations in the stable atmospheric boundary layer using wavelet methods. Bound.-Layer Meteorol. 114, 489–518.

Thistle, H.W., Strom, B., Strand, T., Lamb, B.K., Edburg, S., Allwine, G., Peterson, H.G., 2011. Atmospheric dispersion from a point source in four southern pine thinning scenarios: basic relationships and case studies. Trans. ASABE 54, 1219–1236.

Thomas, C.K., 2011. Variability of Sub-Canopy Flow, Temperature, and Horizontal Advection in Moderately Complex Terrain. Bound.-Layer Meteorol. 139, 61–81. doi:10.1007/s10546-010-9578-9

Thomas, C.K., Martin, J.G., Law, B.E., Davis, K., 2013. Toward biologically meaningful net carbon exchange estimates for tall, dense canopies: Multi-level eddy covariance observations and canopy coupling regimes in a mature Douglas-fir forest in Oregon. Agric. For. Meteorol. 173, 14–27. doi:10.1016/j.agrformet.2013.01.001

Torrence, C., Compo, G.P., 1998. A Practical Guide to Wavelet Analysis. Bull. Am. Meteorol. Soc. 79, 61–78.

Van Gorsel, E., Christen, A., Feigenwinter, C., Parlow, E., Vogt, R., 2003. Daytime turbulence statistics above a steep forested slope. Bound.-Layer Meteorol. 109, 311–329.

Vickers, D., Mahrt, L., 2003. The cospectral gap and turbulent flux calculations. J. Atmospheric Ocean. Technol. 20, 660–672.

Vickers, D., Mahrt, L., 1997. Quality Control and Flux Sampling Problems for Tower and Aircraft Data. J. Atmospheric Ocean. Technol. 14, 512–526.

Williams, A.G., Chambers, S., Griffiths, A., 2013. Bulk Mixing and Decoupling of the Nocturnal Stable Boundary Layer Characterized Using a Ubiquitous Natural Tracer. Bound.-Layer Meteorol. 149, 381–402. doi:10.1007/s10546-013-9849-3

Yue, W., Meneveau, C., Parlange, M.B., Zhu, W., van Hout, R., Katz, J., 2007. A comparative quadrant analysis of turbulence in a plant canopy. Water Resour. Res. 43. doi:10.1029/2006WR005583

Figures

Figure 1. Four- panel plot showing the location of the field site with a white arrow (upper left), and a closer view of the site with the SODAR location also marked with a white arrow (lower left). The right column shows the site before any thinning occurred (UT, upper right) and after the third thinning (T3, bottom right).

Figure 2. Surface weather maps for 7am EST for the first four days of the study period from NOAA's Daily Weather Map series. The blue triangle in Louisiana represents the general area of the field site.

Figure 3. Vertically plotted SODAR data for wind speed (left column) and wind direction (right column) as an average for each thinning period (top row) and each day (bottom row). The black lines in the daily legend indicate the thinning periods starting with UT to T3.

Figure 4. Distribution of the u (a, b), v (c, d), and w (e, f) wind components at 0.13h (left) and 1.13h (right) for each stand density.

Figure 5. Vertical profile of u (a), v (b), w (c), σ_u (d), σ_v (e), and σ_w (f) for all 4 stand densities.

Figure 6. Comparison between the SODAR mean wind speed and the tower-measured friction velocity (u_*, left column) and mean horizontal wind speed (V, right column) for each 30-minute data point (circles) and averaged for each thinning period (x's) at each height.

Figure 7. Three different stability components for UT and T1 (a, c, and e) and T2 and T3 (b, d, and f) for the layer between 0.13h and 0.83h (filled circles) and 0.83h and 1.13h (x markers). Top row (a and b) is the vertical temperature gradient (dT/dz); middle row (c and d) is z/L, where z is the measurement height and L is the Obukhov length, and the bottom row (e and f) is the flux Richardson number (Ri_f).

Figure 8. Scatter plot between the vertical temperature gradient through the whole layer ([$\Theta_{1.13h} - \Theta_{0.83h}$] for 1.13h and [$\Theta_{0.83h} - \Theta_{0.13h}$] for 0.83h and 0.13h) (a, c, and e) and local z/L (b, d, and f) compared to σ_w at 1.13h (a and b), 0.83h (c and d), and 0.13h (e and f).

Figure 9. Vertical profile of u_* (a) and family portrait of the vertical profile: b) streamwise wind (V) normalized by streamwise at 1.13h (V_H), c) σ_w/u_*; d) σ_V/u_*; e) $\overline{w'V'}/u_*^2$; f) R_{wV}. The normalization value for 6b-6e were the relevant value at 1.13h. The shading is the range of values reported in studies cited in the text.

Figure 10. Mean global wavelet spectra for the four different thinning conditions (colors) and the three different heights (1.13h: a, d, and g, 0.83h: b, e, and h, and 0.13h: c, f, and i) over the course of the study period for each wind component (u: top row, a-c; v: middle row, d-f; and w: bottom row, g-i).

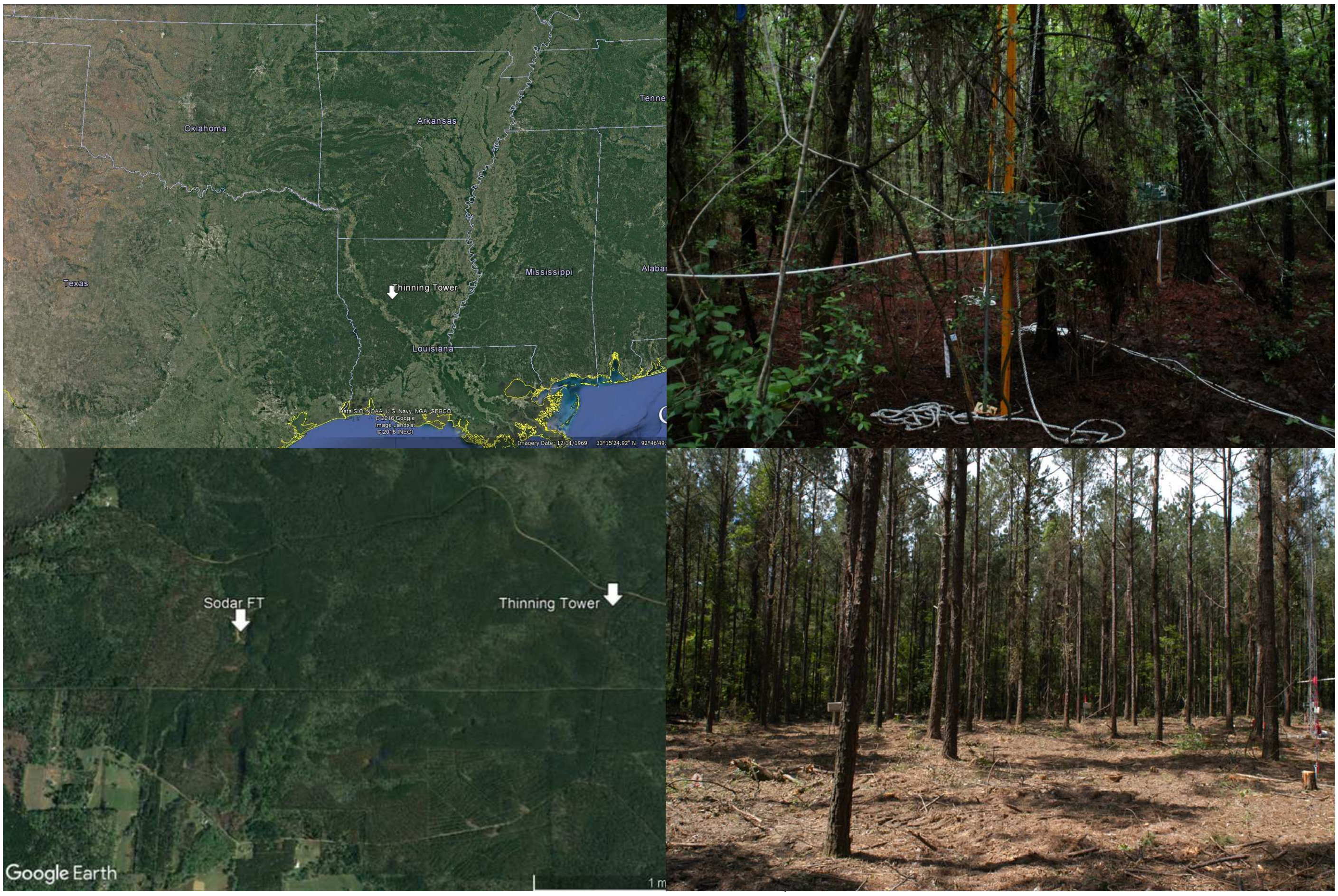

Figure 1. Four- panel plot showing the location of the field site with a white arrow (upper left), and a closer view of the site with the SODAR location also marked with a white arrow (lower left). The right column shows the site before any thinning occurred (UT, upper right) and after the third thinning (T3, bottom right).

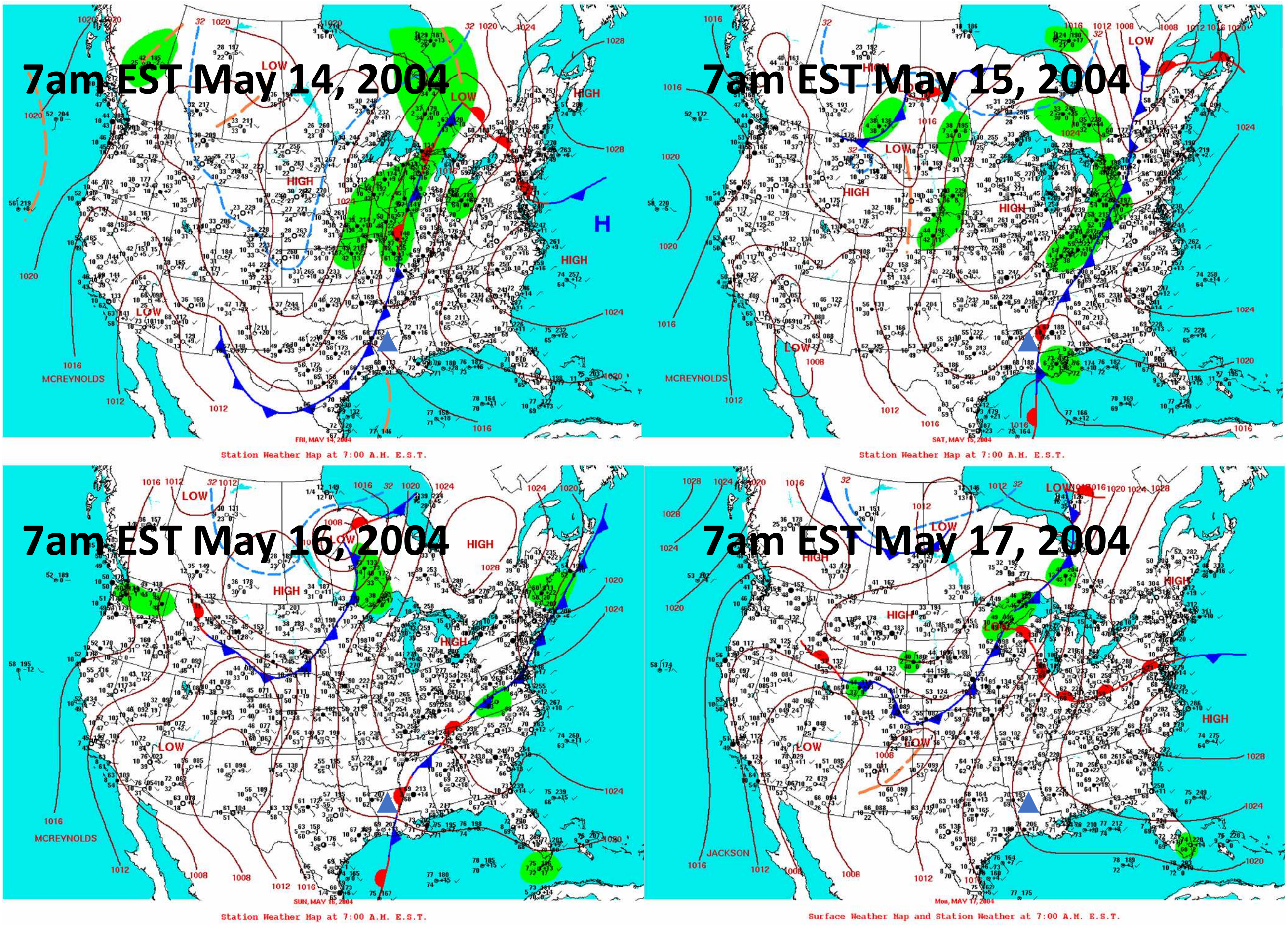

Figure 2. Surface synoptic maps at 7 am EST for the first four days of the study period (Source: NOAA's Daily Weather Map series, http://www.wpc.ncep.noaa.gov/dailywxmap/). The blue triangle in Louisiana represents the general area of the field site.

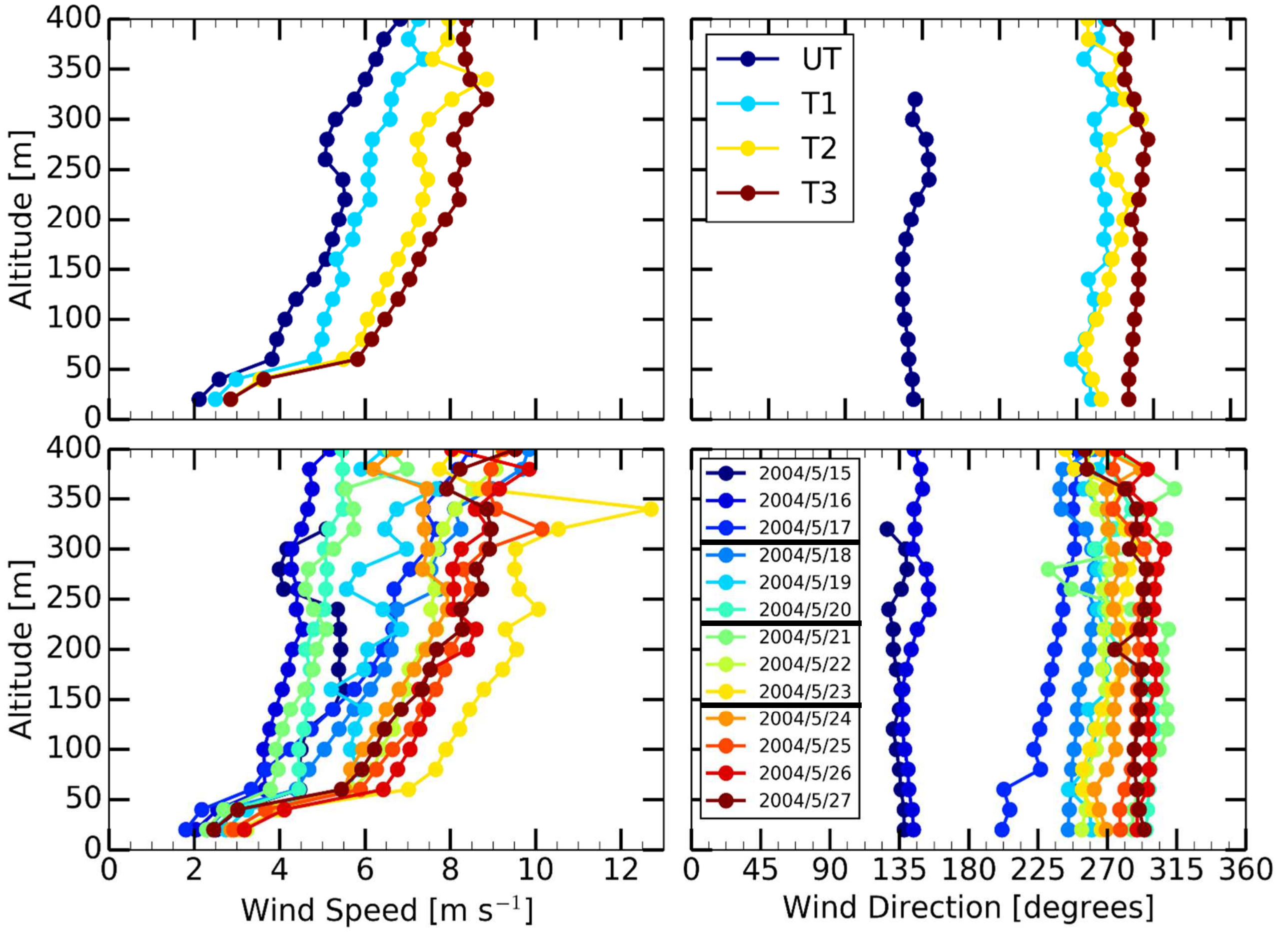

Figure 3. SODAR data showing the vertical profiles of wind speed (left column) and wind direction (right column) as an average for each thinning period (top row) and each day (bottom row). The black lines in the daily legend indicate the thinning periods starting with UT to T3.

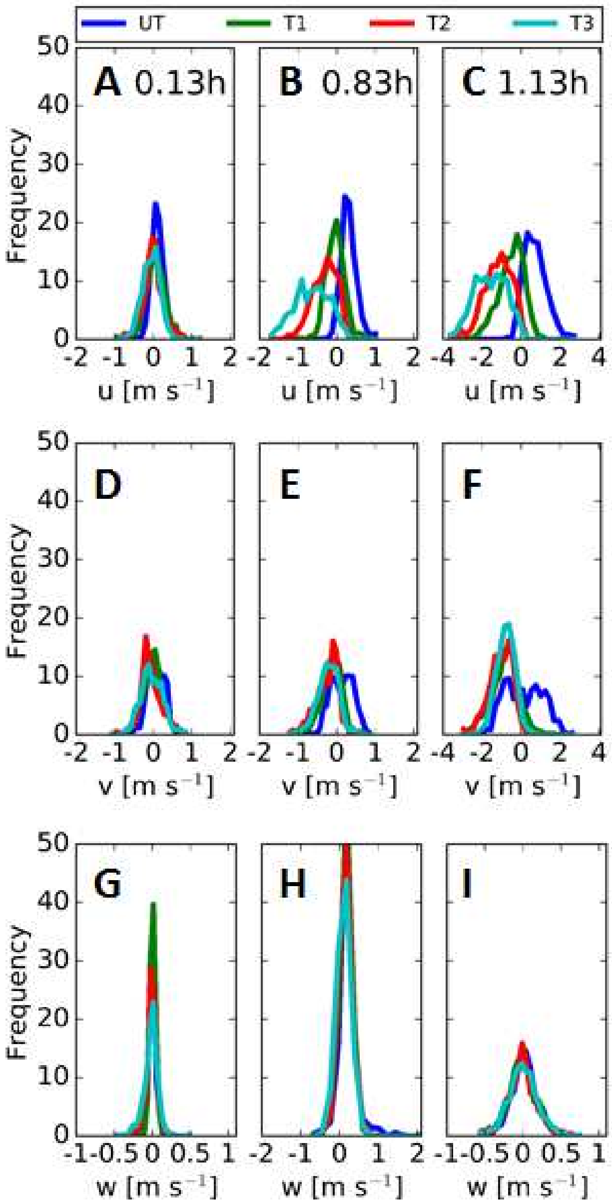

Figure 4. Distribution of the *u* (a, b, c), *v* (d, e, f), and *w* (g, h, i) wind components at 0.13h (left), 0.83h (middle) and 1.13h (right) for each stand density.

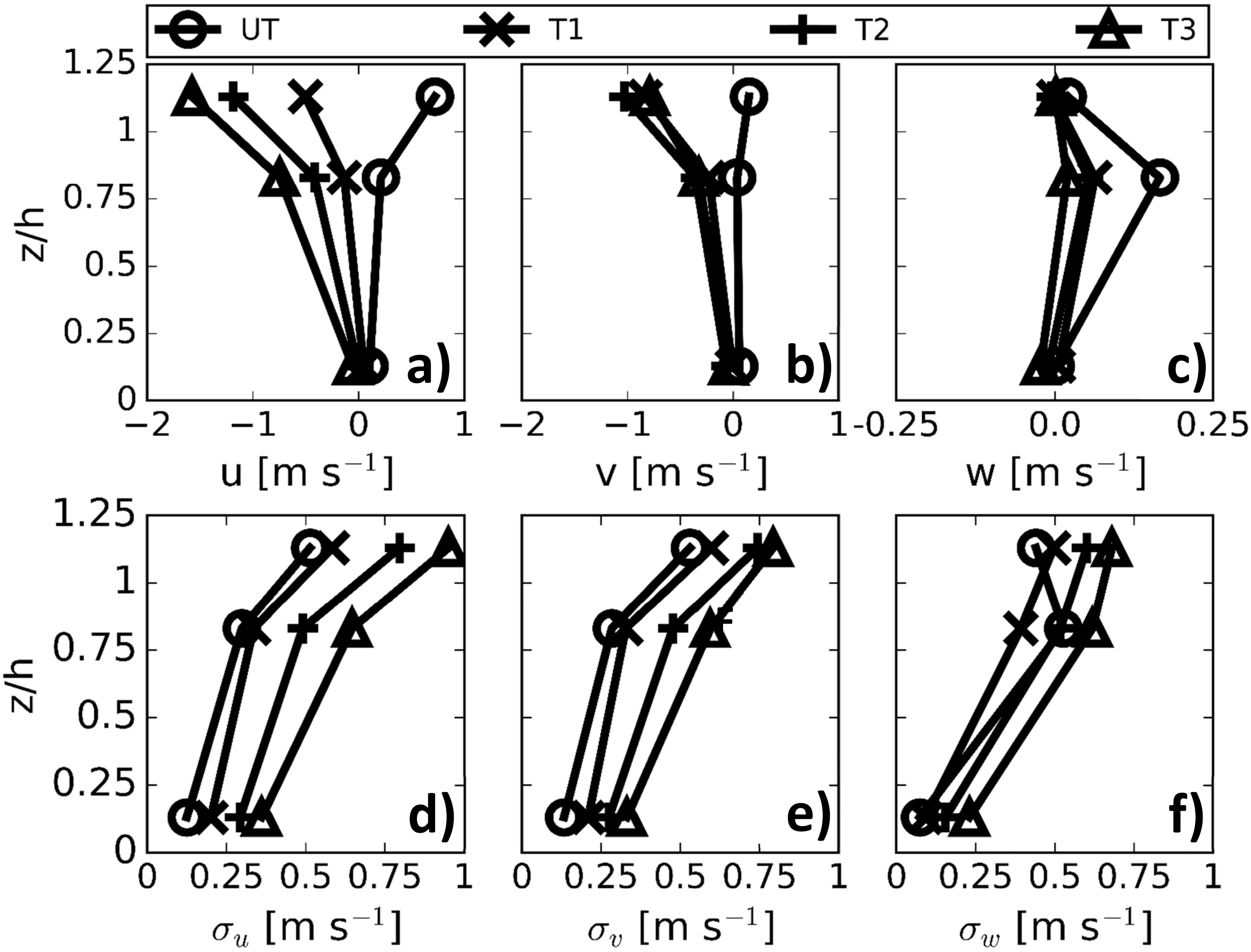

551 **Figure 5.** Vertical profile of u (a), v (b), w (c), σ_u (d), σ_v (e), and, σ_w (f) for all 4 stand densities.
552